COLUMBIA UNIVERSITY

IN THE CITY OF NEW YORK

SCHOOL OF ENGINEERING AND APPLIED SCIENCE

ELECTRONICS RESEARCH LABORATORIES

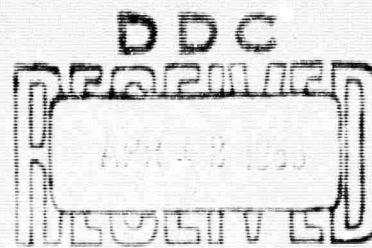# ELECTRO-OPTICAL SIGNAL PROCESSING TECHNIQUES

FOR PHASED ARRAY ANTENNAS

QUARTERLY PROGRESS REPORT P-1/321

OCTOBER 1, 1964 TO DECEMBER 31, 1964

D D C

COLUMBIA UNIVERSITY

IN THE CITY OF NEW YORK

SCHOOL OF ENGINEERING AND APPLIED SCIENCE
ELECTRONICS RESEARCH LABORATORIES

632 WEST 125th STREET

NEW YORK, NEW YORK 10027

CU-3-65-AF-1478-ERL

ELECTRO-OPTICAL SIGNAL PROCESSING TECHNIQUES

FOR PHASED ARRAY ANTENNAS

QUARTERLY PROGRESS REPORT P-1/321

OCTOBER 1, 1964 TO DECEMBER 31, 1964

ABSTRACT

The results of the electro-optical phased array signal processor research program during the past period are presented.

The spatially multiplexed system experimental response for a weighted and unweighted aperture distribution is shown graphically and with photographs. The theoretical and experimental system response for a Hamming type aperture weighting function to signals on and off boresight is presented. An experimental sidelobe suppression of 28 db is demonstrated. A Schlieren photograph of the ultrasonic beams within the light modulator is included.

The time multipex system signal simulator implementation and block diagram are presented. The method utilized for phase alignment of the simulator is discussed.

AUTHORIZATION

The work described in this report was performed at the Electronics Research Laboratories of the School of Engineering and Applied Science of Columbia University. This report was prepared by M. Arm, A. Aimette I. Lambert and N. Wyman.

This project is directed by the Advanced Research Projects Agency of the Department of Defense and is administered by the Air Force Office of Scientific Research under Contract AF 49(638)-1478.

Submitted by: Approved by:

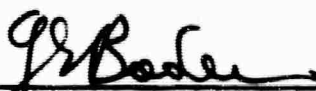L. Lambert   R. A. Bernstein
Laboratory Supervisor   Professor of Electrical
                                       Engineering
                                       Acting Director

TABLE OF CONTENTS

LIST OF FIGURES

LIST OF FIGURES (CONT'D.)

I. INTRODUCTION

The distinguishing characteristic of the spatially mul-
tiplexed system is that it utilizes one ultrasonic channel
for each element of the linear array. The input signal to
each transducer therefore possesses the relative phase in-
formation corresponding to the angular location of the tar-
get wave front impinging upon the array. By employing the
signals of each element to spatially modulate a coherent
beam of light and optically forming the far-field pattern of
the modulated beam in a plane, the resulting light intensity
distribution in that plane is the direct optical analogue of
the far-field of the antenna.

The physical location of the light distribution peak
intensity in this plane corresponds to the angle of signal
arrival at the array. Note, however, that the processor **does
not** quantize angular coverage in either space or time: all
angles are examined simultaneously and continuously. The
theoretical capabilities (3-db resolution width, side lobe
suppression, and dynamic range) of the spatially multiplexed
system have been shown[1] to be identical to the intrinsic
characteristics of the phased array: the processor does not
degrade the performance of the linear array.

A spatially multiplexed system with the capability of
processing the output of a 24-element array has been de-
signed and constructed. The system has been thoroughly des-
cribed previously;[2] a brief description of the system will
be repeated here.

---

[1] For numbered references see Sec. IV.

Figure 1 shows the spatially multiplexed electro-optical signal processor system.

The He-Ne laser, together with the divergent lens, the collimator lens, and the aperture stop provide the plane collimated light for the system. The input light beam is then divided into 24 parallel beams by the channel separator mask; these 24 beams then pass through the ultrasonic cell. The 20-mc signal input to each transducer, corresponding to a single linear array element output is generated in the signal simulator by a separate, variable phase, amplifier-driver. The 24-output light beams of the light modulator are therefore individually phase modulated in accordance with the phase characteristic of a simulated signal arriving at the antenna array. The output beams pass through the integration lens and are focused in the output focal plane. The light intensity distribution in this plane, corresponding to the Fourier transform of the modulated light output of the cell, is then scanned by a 1-micron slit; the output of this slit is converted to a dc voltage by a photomultiplier tube. The photomultiplier output and a calibrated position voltage are simultaneously fed to the x-y recorder.

The graphical output of the recorder presents the logarithm of the light intensity distribution in the output focal plane corresponding to the Fourier transform of the modulated light output of the ultrasonic cell. Therefore the light output distribution as shown on the recorder is the optical analogue of the far-field pattern of the antenna array. By measuring the positions of the peaks in this light distribution the angular location of all targets which contributed to the antenna illumination pattern can be established.

The theory and development of the electro-optical system operating in the spatially multiplexed mode has been
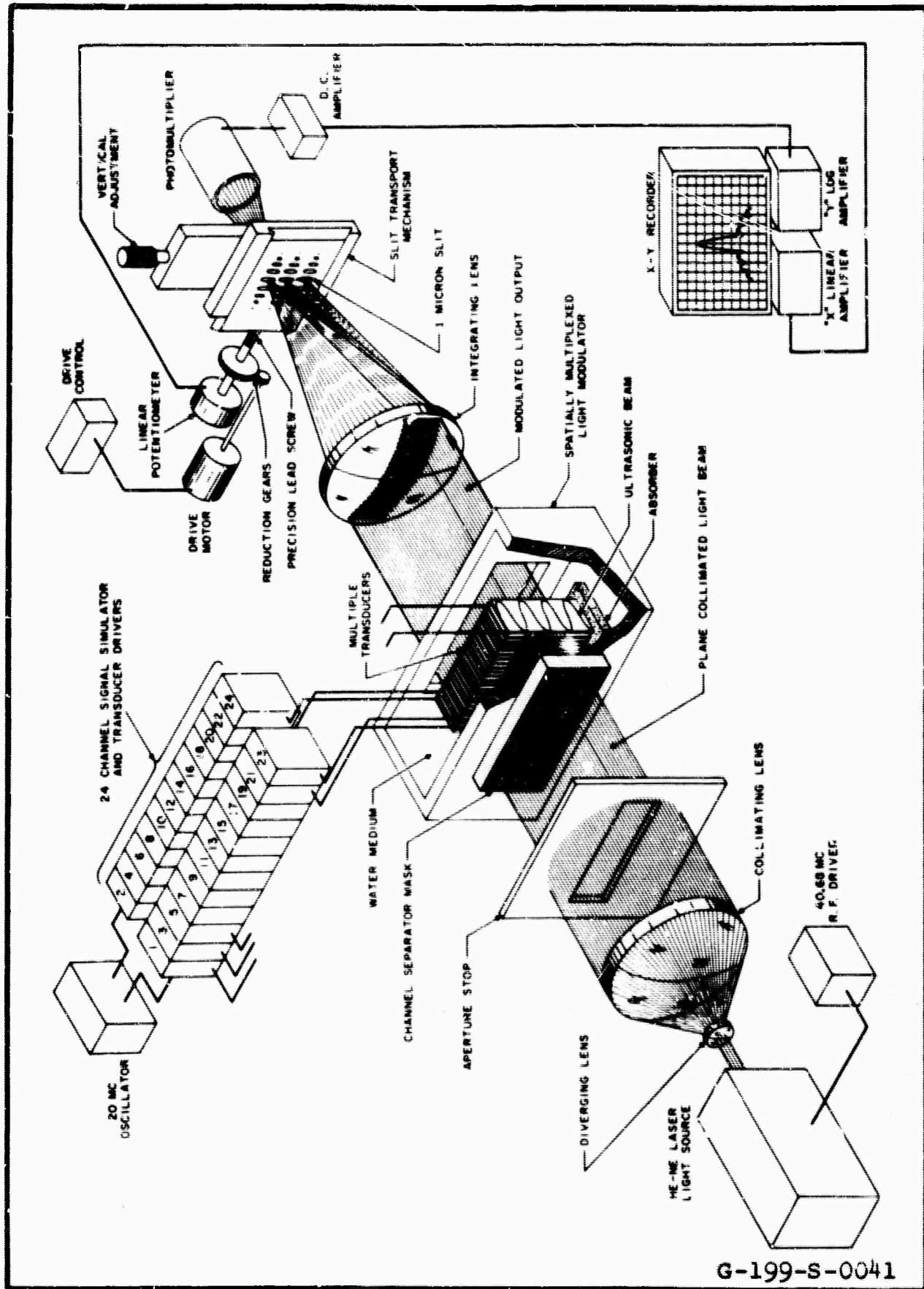
Fig. 1 Spatially Multiplexed Electro-Optical
Signal Processor

developed previously.[1,2] The experimental results presented have shown that the spatially multiplexed system response when processing the output of a simulated, uniformly weighted linear antenna array is very nearly ideal. The resolution, the sidelobe level and dynamic range obtainable with this experimental system demonstrates the engineering feasibility of this mode of operation and the capability of the device to process the output of uniformly weighted antenna arrays.

This report presents the extension of the previous results to processing the simulated signal output of an amplitude weighted antenna array.

II. THE SPATIALLY MULTIPLEXED SYSTEM

A. SYSTEM THEORY: THE PROCESSOR AS AN ANALOGUE SYSTEM

The theoretical basis for the electro-optical processor has been thoroughly discussed in previous reports of this research program. It is useful here to repeat the results which are applicable to the program of this past period.

As a consequence of the theorem of reciprocity the radiation patterns of a linear array when receiving and transmitting are identical. The far-field pattern is related to the amplitude and phase distribution across the aperture (the elements) of the array by the Fourier transform. If $A(x)$ and $\phi(x)$ are the functions specifying these distributions in the aperture then,

$$F_t[A(x)e^{j\phi(x)}] = K_1 A(x')e^{j\phi(x')} = K_2 A(\theta)e^{j\phi(\theta)} \quad (1)$$

states this relation. Here x, x', and θ are the aperture coordinate, the far-field coordinate, and the off-boresight axis angle, respectively.

For a uniform amplitude and a linear phase distribution across the array aperture, the radiation intensity pattern for an array of N elements, spaced d apart, and operating at λc wavelength can be shown to be given by

$$G(\theta) = G_e(\theta) \frac{Sin^2\left[N\pi\left(\frac{d}{\lambda c}\right)\left(Sin\ \theta - Sin\ \theta_o\right)\right]}{Sin^2\left[\pi\left(\frac{d}{\lambda c}\right)\left(Sin\ \theta - Sin\ \theta_o\right)\right]} \quad (2)$$

where $G_e(\theta)$ is the radiation pattern of an individual element of the array. The maxima of the pattern is at an angle θ_0 off the boresight axis. The 3-db beamwidth is given by

$$\Delta\theta_{3\,db} = \frac{0.886\lambda c}{N_d \cos\theta_0} \tag{3}$$

For the spatially multiplexed system shown in Fig. 1 the light intensity distribution in the plane of the slit transport mechanism (the output focal plane) is related to the amplitude and phase distribution of the modulated light in the aperture by a Fourier transform and is given by

$$I_N(\theta) = K_2\, I(\theta)\, \cdot$$
$$\frac{\sin^2\left[N\pi\left(\dfrac{d}{\lambda c}\right)\left(\sin\theta - \sin\theta_0\right)\right]}{\sin^2\left[\pi\left(\dfrac{d}{\lambda c}\right)\left(\sin\theta - \sin\theta_0\right)\right]} \tag{4}$$

for the conditions of uniform amplitude and linear phase distribution. $I(\theta)$ is the light intensity distribution of one channel of the processor. The 3-db beamwidth is given by

$$\Delta\theta_{3\,db} \doteq \frac{.886\lambda c}{N_d \cos\theta_0} \tag{5}$$

For nominal excursions of θ, $|\theta| < 60°$ both $I(\theta)$ and $G_e(\theta)$ vary slowly. The systems are therefore analogous and possess identical characteristics. Note also that since the systems are linear, multiple targets appear as separate outputs.

B. **THE PROCESSOR EQUATIONS**

The relative intensity distribution in the output focal plane of the system corresponding to a uniform aperture dis-

tribution and a single target at an angle θ can be approximated by

$$I(x',y') \doteq |E_0(x',y')|^2 + |E_{+1}(x',y')|^2 + |E_{-1}(x',y')|^2 \quad (6)$$

where

$$|E_0(x',y')|^2 = K_1 \operatorname{Sinc}^2 \frac{Dx'}{\lambda_L F} \left[\frac{\operatorname{Sin} \frac{\pi N \ell y'}{\lambda_L F}}{\operatorname{Sin} \frac{\pi \ell y}{\lambda_L F}}\right]^2 \cdot \operatorname{sinc}^2 \frac{\omega y'}{\lambda_L F} \quad (6a)$$

and

$$|E_{\pm 1}(x',y')|^2 = k_2 \operatorname{Sinc}^2 D\left(\frac{x}{\lambda_L F} \mp \frac{f_0}{s}\right) \cdot$$

$$\left[\frac{\operatorname{Sin} \pi N \ell \left(\frac{y'}{\lambda_L F} \pm \frac{d}{\lambda_c \ell} \operatorname{Sin} \theta\right)}{\operatorname{Sin} \pi \ell \left(\frac{y'}{\lambda_L F} \pm \frac{d}{\ell \lambda_c} \operatorname{Sin} \theta\right)}\right]^2 \cdot \operatorname{Sinc}^2 \frac{\omega y'}{\lambda_L F} \quad (6b)$$

where

$(x',y') \equiv$ focal plane coordinates

$(D,L) \equiv$ the (x,y) aperture dimensions

$\lambda_L \equiv$ light wavelength

$\lambda_c \equiv$ antenna operating wavelength

$f_0 \equiv$ operating frequency of light modulator (intermediate frequency)

$s \equiv$ ultrasonic velocity of propagation

$F \equiv$ focal length of the integration lens

$d \equiv$ array element spacing

$\theta \equiv$ angle of target off-boresight

$\ell \equiv$ ultrasonic transducer spacing

W $\equiv$ ultrasonic transducer width

N $\equiv$ number of elements, $L \equiv N\ell$

$K_1, K_2 \equiv$ normalizing constants

Equation 6 shows that there are three major intensity distributions, or fringes, in the plane, $|E_o|^2$ the zero order fringe and $|E_\pm|^2$ the positive and negative first order fringes respectively. The zero and first order fringes differ only in the location and magnitude of their peak intensity; the zero order maxima is located at $(0, 0)$ and the peaks of the first order fringes at $(\pm \lambda_L F f_o/s, \mp d\lambda_L F/\ell\lambda_c \sin \theta)$, are functions of θ the angle of arrival of the signal and the ultrasonic frequency f_o. However only one of the first order fringes need be considered since both contain the same target angle information.

Consider the positive first order fringe intensity distribution normalized with respect to its peak value

$$\left| E_1\left(x^1 \equiv \frac{\lambda_L F f_o}{s}, y'\right)\right|^2_{Norm} =$$

$$K_3 \; \text{Sinc}^2 \frac{\omega y'}{\lambda_L F} \; \frac{\text{Sin}^2 \; \pi N\ell\left(\frac{y'}{\lambda_L F} + \frac{d}{\ell\lambda_c} \sin \theta\right)}{\text{Sin}^2 \; \pi\ell\left(\frac{y'}{\lambda_L F} + \frac{d}{\ell\lambda_c} \sin \theta\right)} . \quad (6c)$$

Consider the case where $\theta = 0$, target on boresight. The second term of Eq. (6c) will then have principal maxima at $y' = 0, \pm \lambda_L F/\ell, \pm 2\lambda_L F/\ell + \ldots\ldots + n\lambda_L F/\ell$. These maxima or fringes may be conveniently designated as the $(+ 1, \pm n)$ fringes and their peak intensity is given by

$$K_3 \; \text{Sinc}^2 \frac{n\omega}{\ell} . \quad (7)$$

When the target angle θ varies over $\pm 90^{\circ}$ the position of the $(+1, \pm n)$ fringes vary over the range $\mp d\lambda_L F/\lambda_c \ell$ on either side of their $n\lambda_L F/\ell$ positions. It is therefore sufficient to restrict the region of interest to $|y'| \leq d\lambda_L F/2\lambda_c \ell$ and find the position of the $(+1, 0)$ fringe since the $(+1, \pm n)$, $n > 0$, fringes are suppressed by a suitable choice of the weighting function (Eq. 7).

The 3-db width of the first order fringes can be shown to be given by

$$\Delta y'_{3 \text{ db}} = \frac{0.886}{N\ell} \lambda_L F \tag{8}$$

Along the $(x \,\vert\, y = \text{constant})$ axis the light intensity distribution is proportional (from Eq. 6) to

$$\text{Sinc}^2 \ D\left(\frac{x'}{\lambda_L F} \mp \frac{Kf_o}{s}\right) \tag{9}$$

for the $[(k, n): K = 0, \pm 1, n = 0, \pm 1, \ldots]$ fringes. The 3-db width of these fringes is given by

$$\Delta x'_{3 \text{ db}} = \frac{0.886 \ \lambda_L F}{D} \tag{10}$$

C. APERTURE WEIGHTING

Equations 2 and 4 show that both the antenna and the processor patterns possess sidelobes which reduce the discrimination capabilities of the system. By weighting the amplitude distribution across the aperture a significant reduction of the sidelobe levels is possible.

For simplicity consider the case where the aperture function is continuous and the phase distribution is uniform. If the aperture function is written as

$$T(y) = P_L(y) \tag{11}$$

where

$$P_L(y) \equiv \begin{cases} 1 & |y| \le L \\ 0 & |y| > L \end{cases}$$

and L is the length of the aperture. Then the normalized far-field intensity pattern is given by

$$|F_t[T(y)]|^2 = \text{Sinc}^2 \, Lv \tag{12}$$

where v is a normalized far-field plane coordinate. For this case the sidelobe level, defined by the intensity of highest sidelobe in the pattern, here the first sidelobe, is 13.2 db below the maxima.

If the amplitude distribution is weighted with a Hamming type function such that the aperture distribution is

$$T_a(y) = [a + (1-a) \cos \frac{2\pi}{L} y] \, P_L(y) \tag{13}$$

the sidelobe level can be significantly reduced. For a = 0.54 $T_a(y)$ becomes the Hamming function and a minimum sidelobe level of 42.7 db is possible. The parameter a is related to the relative amplitude at the edges of the aperture, h , by

$$h = 2a - 1 \tag{14}$$

The far-field intensity distribution for the Hamming type aperture weighting is given by

$$|F_t[T_a(y)]|^2 = \text{Sinc}^2 Lv \left[\frac{(2a-1)v^2L^2-a}{a(v^2L^2 - 1)} \right]^2 \tag{15}$$

The sidelobe level as a function of h is shown in Fig. 3. The curve is discontinuous since the sidelobe level is determined by different sidelobes as h varies.

Figure 2 depicts the far-field intensity distribution for the case where $h = 0.2$. Note that the sidelobe level is determined by the second sidelobe and is 31.6 db below the peak of the main lobe. The 3-db width increase for this particular aperture weighting is 30%.

Equation 6b was written for a uniform aperture distribution $(T_a(y)/_{a\equiv 1})$. However in the vicinity of the $(+1, 0)$ fringe peak (within ± 3 sidelobes) the second term can be approximated, assuming $\theta \equiv 0$ for simplicity, by

$$\left[K_2 \frac{\mathrm{Sin}\ \pi N \ell \left(\frac{y'}{\lambda_L F} \right)}{\mathrm{Sin} \frac{\pi \ell y'}{\lambda_L F}} \right]^2 \doteq K_3\ \mathrm{Sinc}^2 \frac{N \ell y'}{\lambda_L F} = \mathrm{Sinc}^2\ Lv \qquad (16)$$

where:

$$v \equiv \frac{y'}{\lambda_L F} \quad \text{and} \quad L \equiv N\ell.$$

Equation 16 thus shows that in the immediate vicinity of the $(+1, 0)$ fringe peak the normalized sidelobe response for the processor is almost identical to that of a continuous aperture of length L. Moreover the maximum sidelobe level in the region of interest of the processor $|v| < 12/L$, is determined by the peak intensity of the first few lobes. Therefore the results of a Hamming type function weighting as derived for the continuous case (Eq. 15) is applicable and may be used to determine the maximum sidelobe level of the processor. For the case shown in Fig. 2, $h = 0.2$, the maximum sidelobe level in the vicinity of the $(+1, 0)$ fringe is reduced from 13.2 db to 31.6 db.
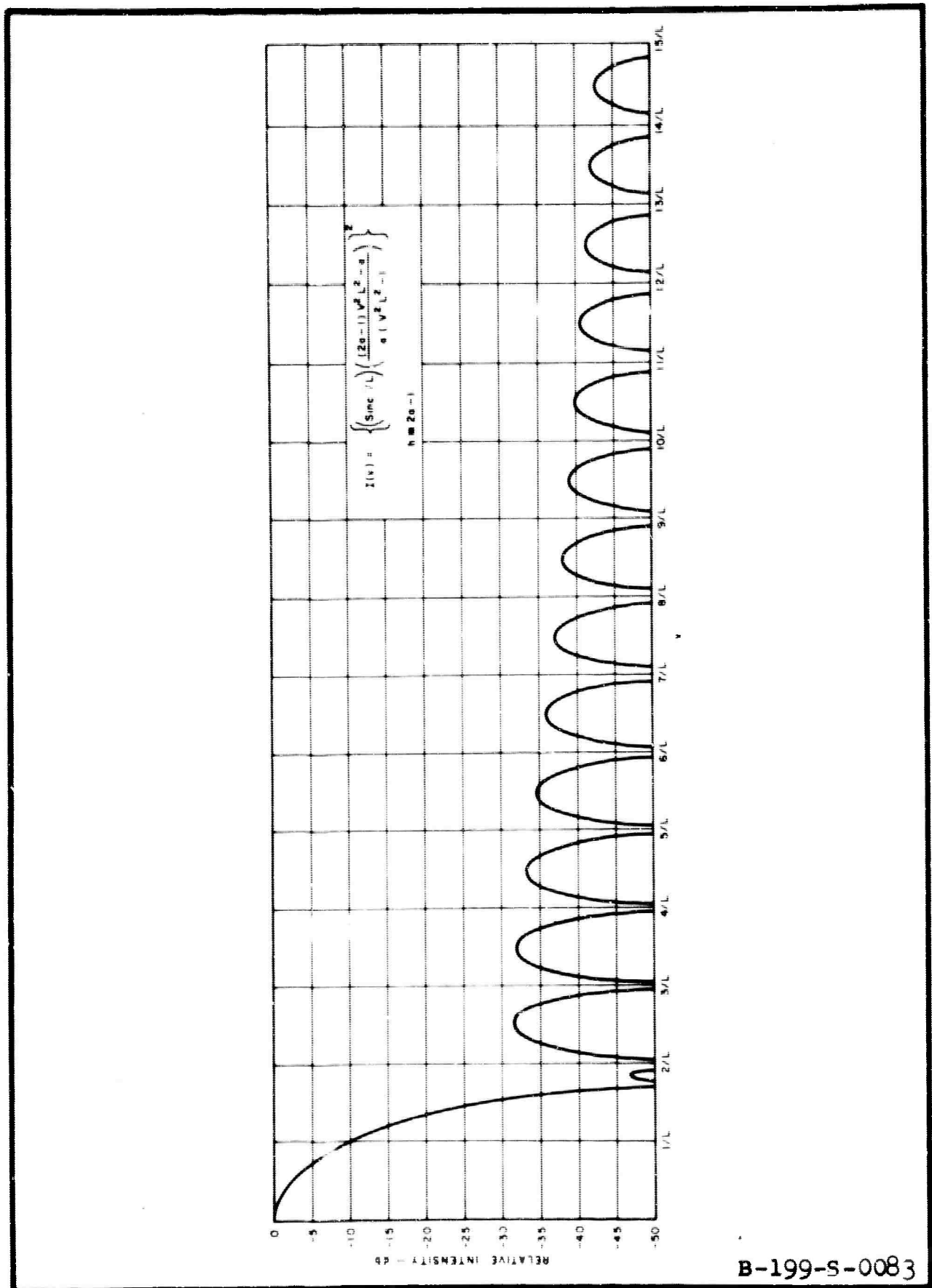
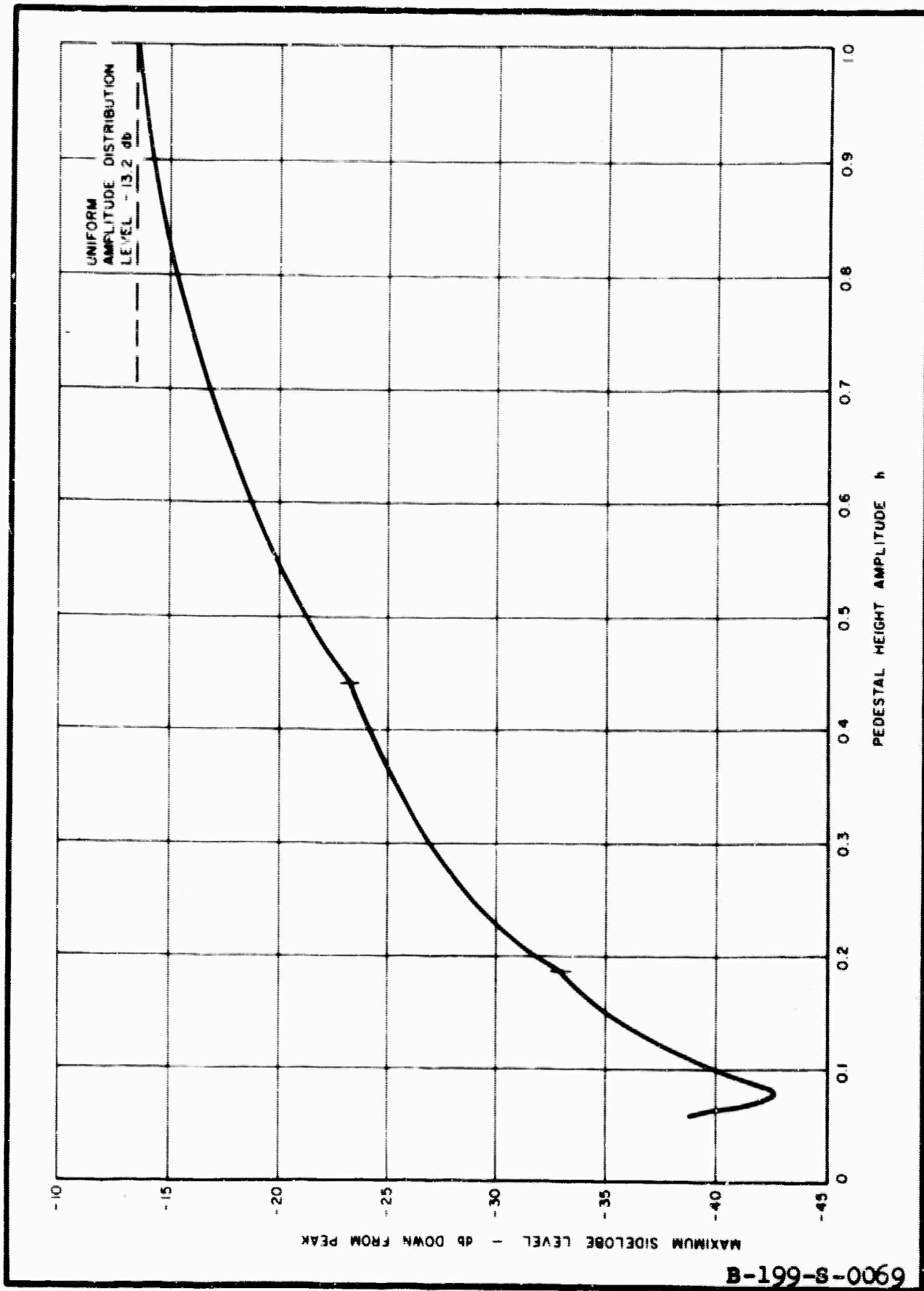Fig. 2 Far Field Intensity Distribution For
Hamming Function Weighting h = 0.2

Fig. 3 Sidelobe Level As Function Of Pedestal Height For The
Hamming Amplitude Weighting Function

P-1/321

-13-

In the following section this weighting function will be applied to the spatially multiplexed system and the experimental system response will be obtained.

D. **EXPERIMENTAL RESULTS - THE ZERO ORDER RESPONSE**

Figures 4, 5 and 6 show the measured Zero Order light intensity distribution for a uniform aperture.

Figure 4 is a photograph of the light intensity distribution (magnification = 100) in the vicinity of the Zero Order fringes, (0, 0), (0, + 1) and (0, - 1), with increasing exposure time. As the exposure time increases the sidelobes in both the x' and y' directions are more clearly visible.

Figures 5 and 6 show the light intensity distributions as obtained with the slit scanning mechanism and recorder shown in Fig. 1. The fine structure of the distribution is clearly shown. The theoretical sidelobe response and the measured half power widths are indicated. Note that the experimental sidelobe maxima are very nearly ideal but some "ripple" or variation in the peak values is evident; the nulls in the vicinity of the main peak go down only 25 db. Since the (+ 1, 0) fringe is essentially a displaced replica of the (0, 0) fringe these results provide a standard of comparison for the system response to a target signal as contained in the first order fringe (+ 1, 0).

E. **EXPERIMENTAL RESULTS - THE WEIGHTED APERTURE**

It was previously shown[1] that the peak intensity of the first order fringes is proportional to the square of the voltage applied to the transducer. Since each transducer input voltage is generated in a separate variable phase, variable gain amplifier, the input voltage and hence the peak intensity of the output focal plane pattern of each transducer can be adjusted independently.
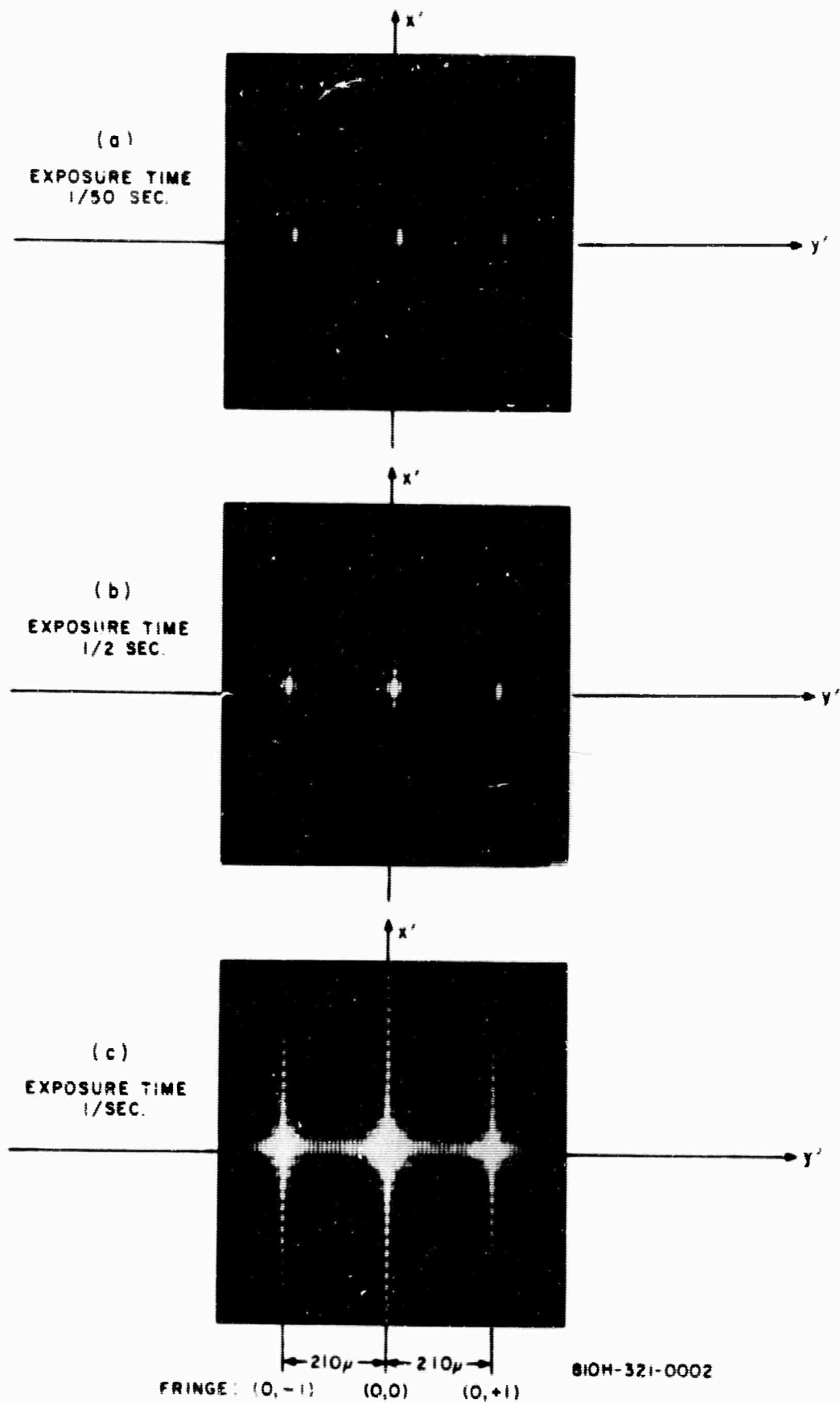
FIG. 4   ZERO ORDER FRINGE LIGHT INTENSITY DISTRIBUTION
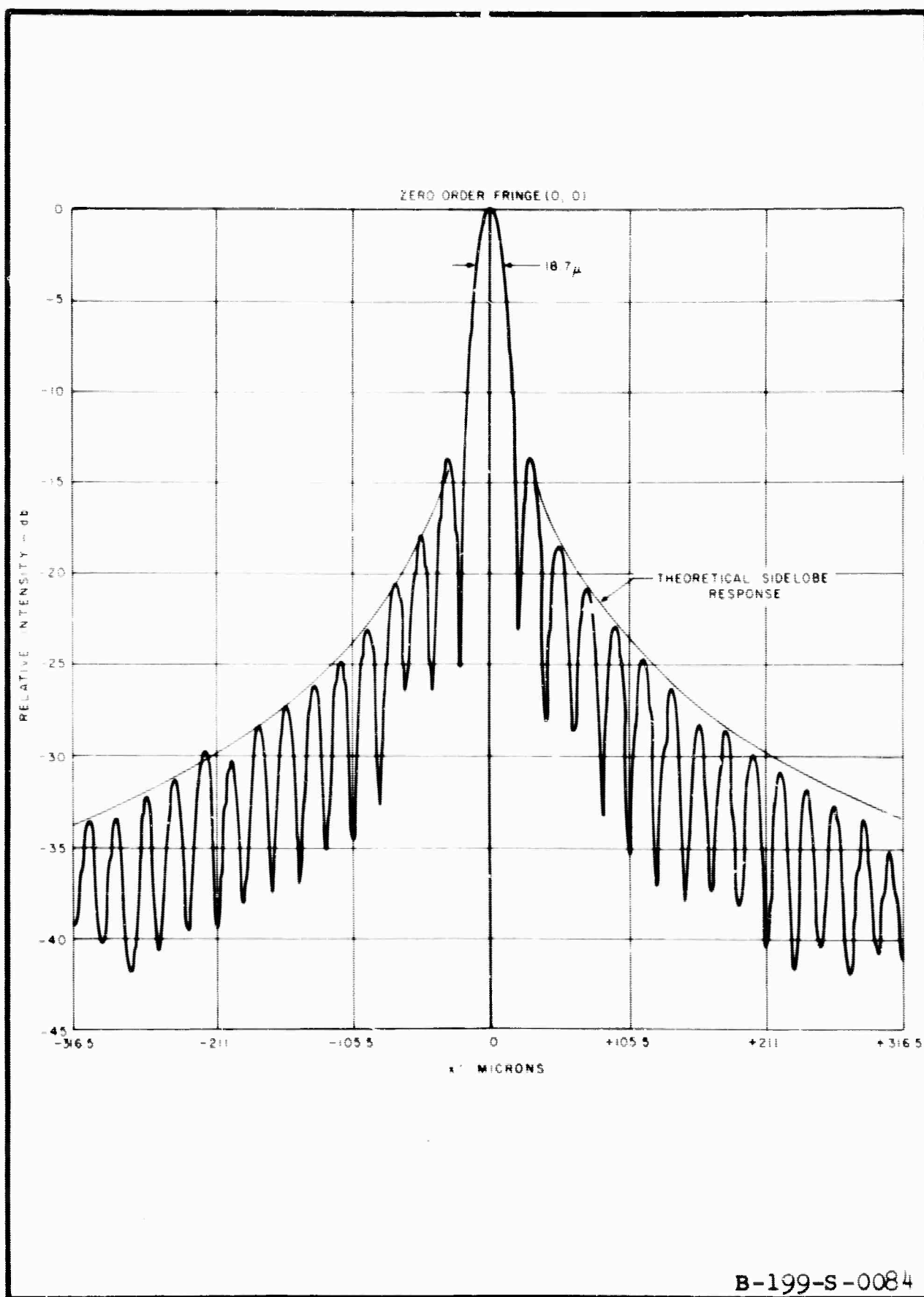AT THE OUTPUT FOCAL PLANE   (MAGNIFICATION x 100)

Fig. 5 Experimental Zero Order Light Intensity Distribution
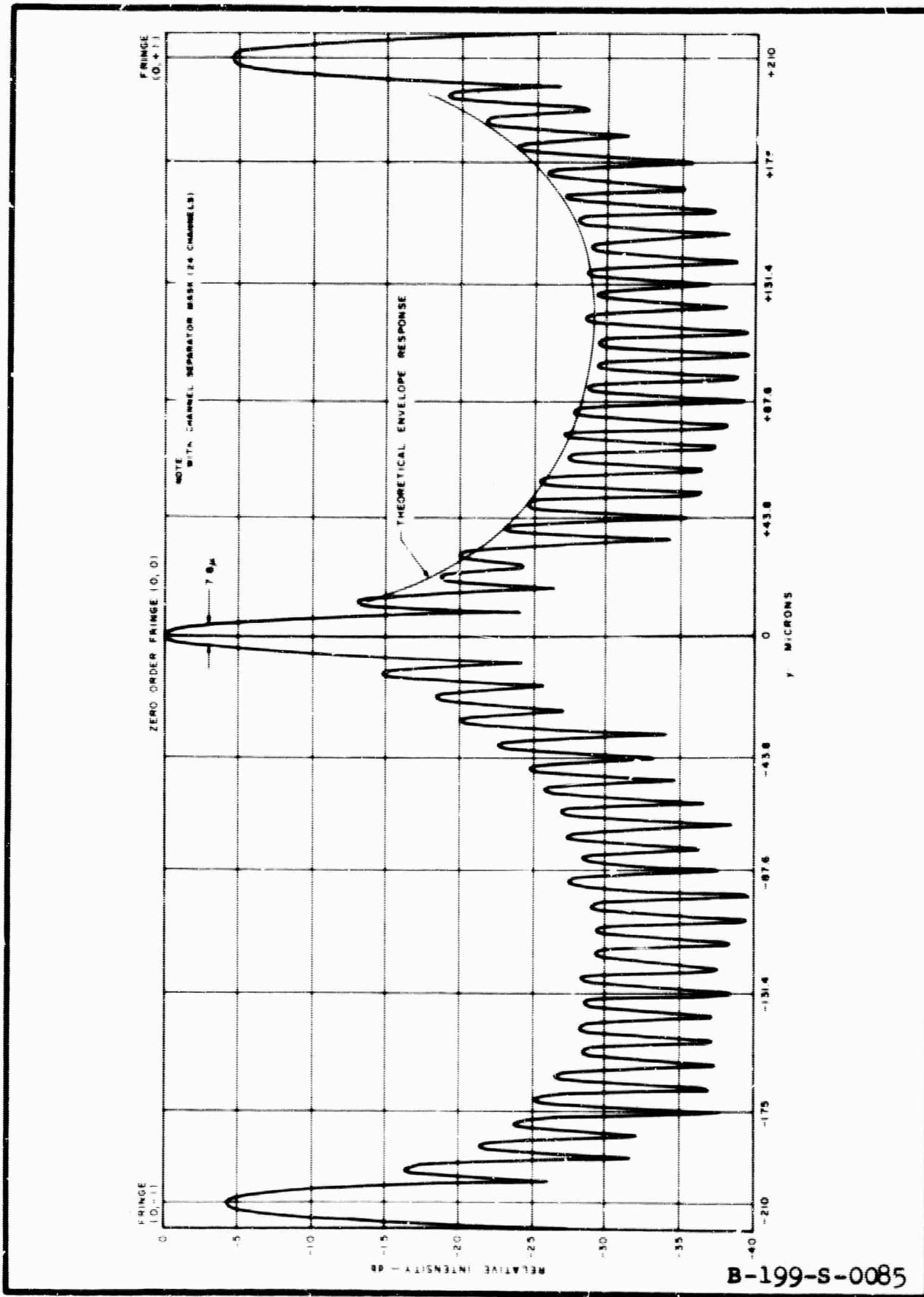In Output Focal Plane - x' Dimension

Fig. 6 Experimental Zero Order Light Intensity Distribution
In Output Focal Plane - y' Dimension

The weighting function chosen was the Hamming type with $h = 0.2$. The sidelobe response for this weighting function is shown in Fig. 2. Since the aperture was not continuous but consists of 24 discrete channels, the amplitude for each transducer was calculated using the center point of the transducer, $y = n\ell$, $n = \pm 1/2, \pm 3/2, \ldots, \pm 23/2$, in Eq. 13. Using these amplitude values, the peak intensity of the corresponding focal plane fringes were calculated. By setting the slit at the $x' = 8440 \mu$, $y' = 0$ point in the focal plane, the peak intensity of each channel was adjusted to the predetermined values defined by the aperture amplitude distribution.

Figure 7 shows the measured light output intensity distribution of each channel. This measurement was obtained by using a ylindrical lens to form the Fourier transform in the x' dimension only. A scanning slit and photomultiplier were then used to obtain the peak value of each channel in the first order fringe along the y' direction. This figure indicates that an amplitude error of about $\pm 2\%$ existed in the aperture amplitude distribution.

Figure 8 shows a Schlieren photograph of the 24 ultrasonic beams within the light modulator. Note that the photograph clearly shows the separate, collimated, ultrasonic beams, with very little coupling between adjacent transducers. The striations which appear between channels are a result of Fresnel diffraction and interference phenomena.

F.   **EXPERIMENTAL RESULTS - THE FIRST ORDER RESPONSE**

Figures 9 and 10 show the measured first order $[(+1, 0), (+1, \pm 1)]$ fringes.

Figure 9a shows a photograph of the output focal plane light intensity distribution in the vicinity of the $(+1, 0)$
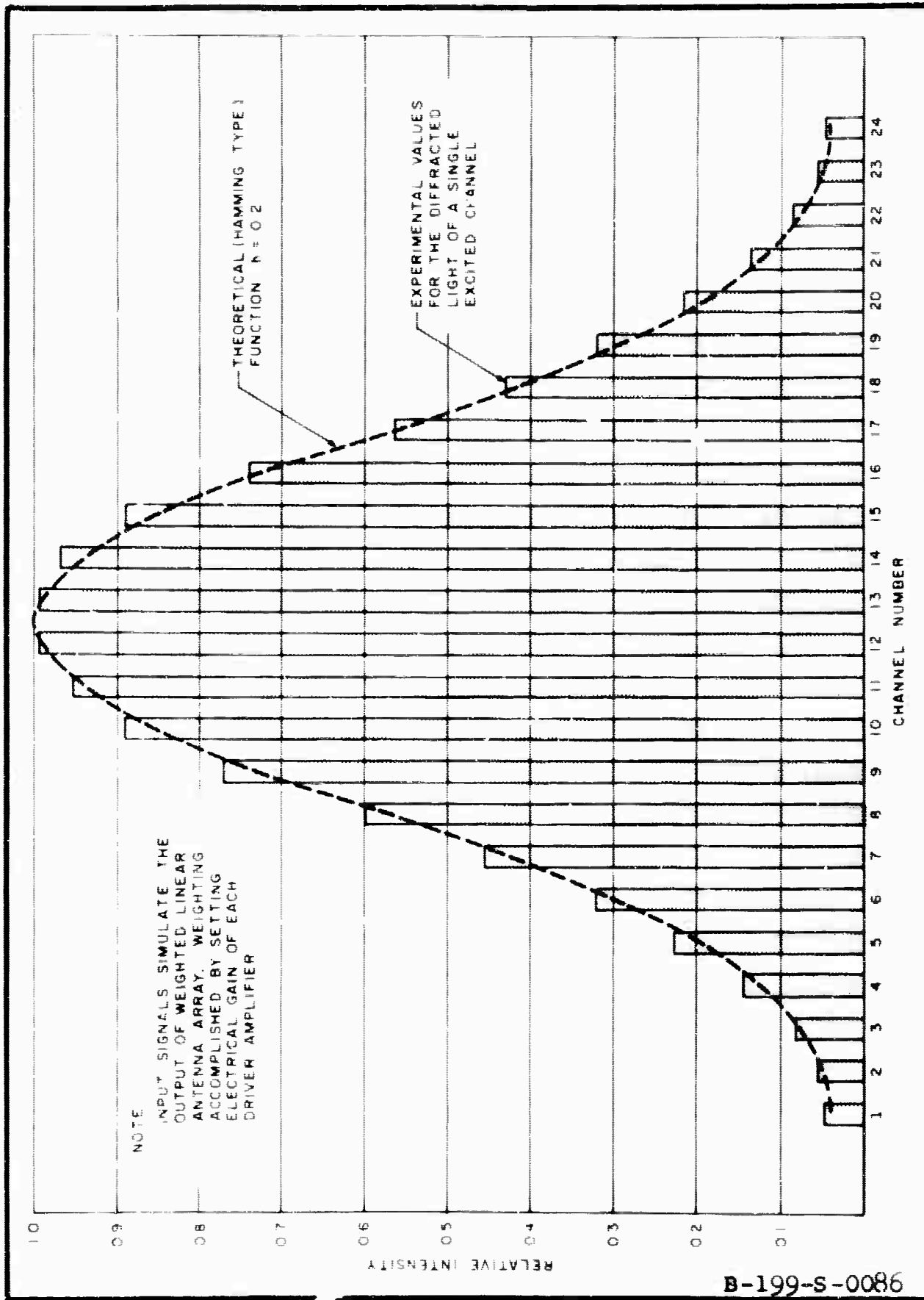
Fig. 7 Measured Light Intensity Across The Aperture For
Sidelobe Suppression By Weighting With A Hamming Type Function
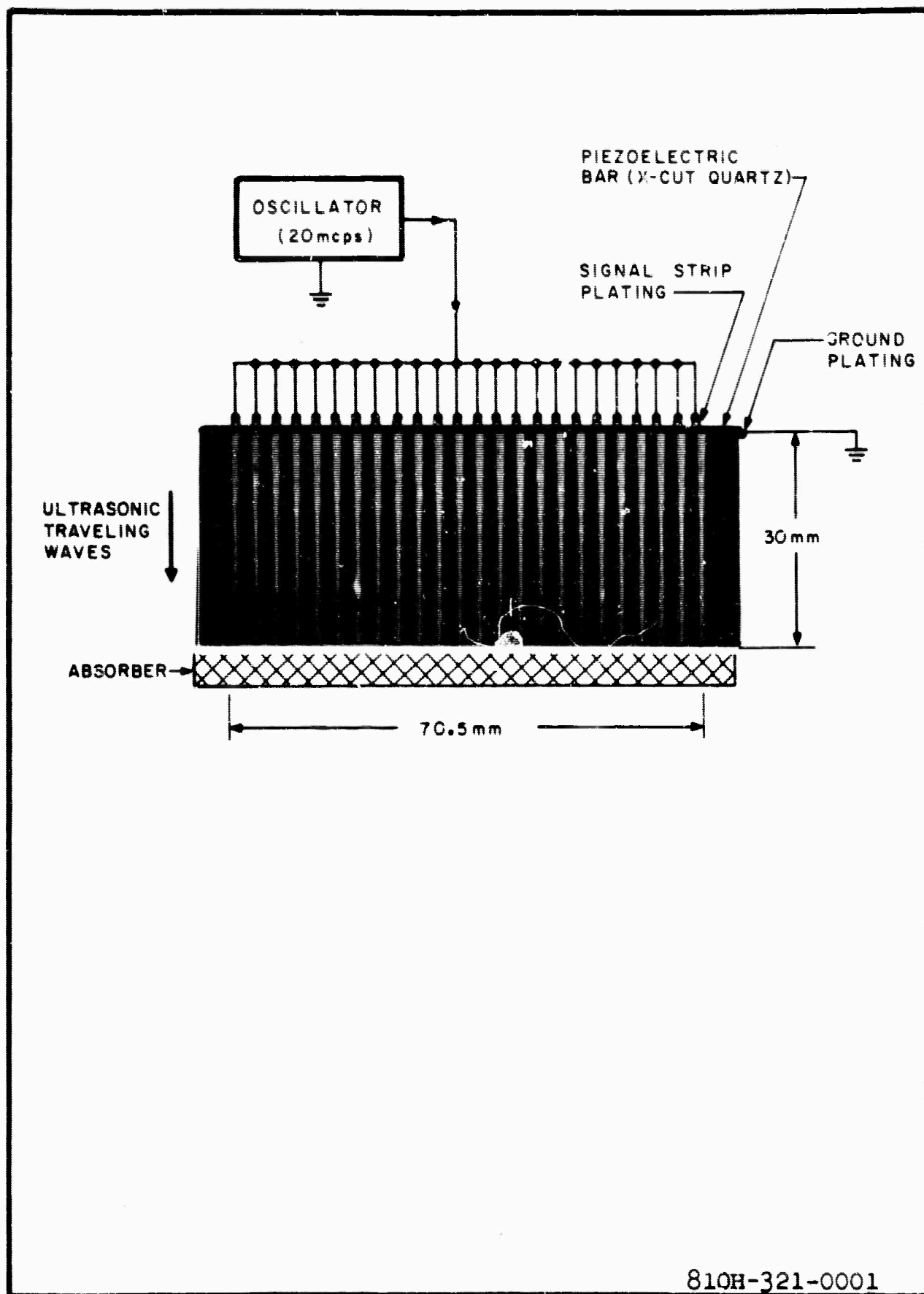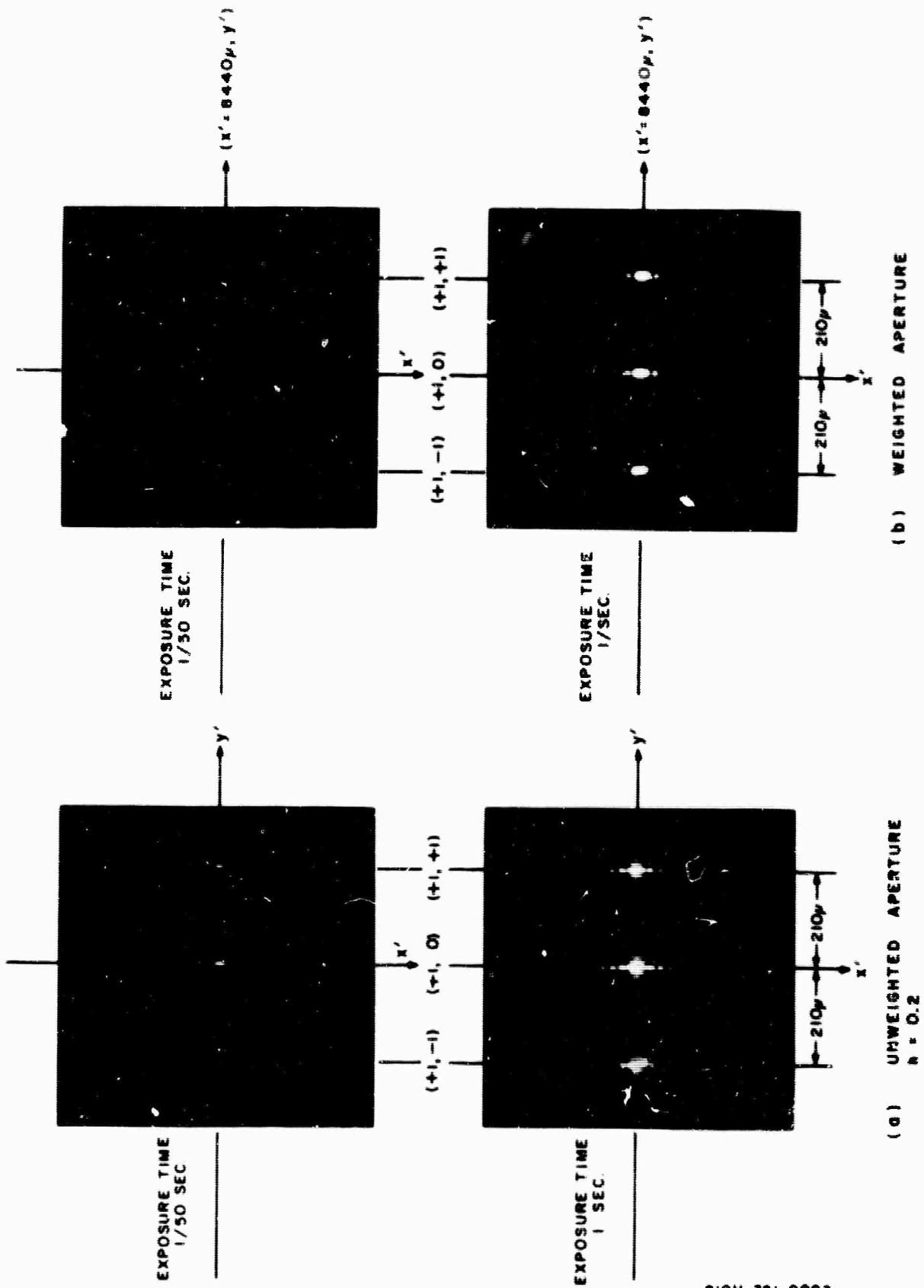
Fig. 8 Experimental Schlieren Photograph: The Formation of
24 Ultrasonic Beams Within The Light Modulator

FIG. 9   FIRST ORDER (SIGNAL) FRINGE LIGHT INTENSITY DISTRIBUTION AT
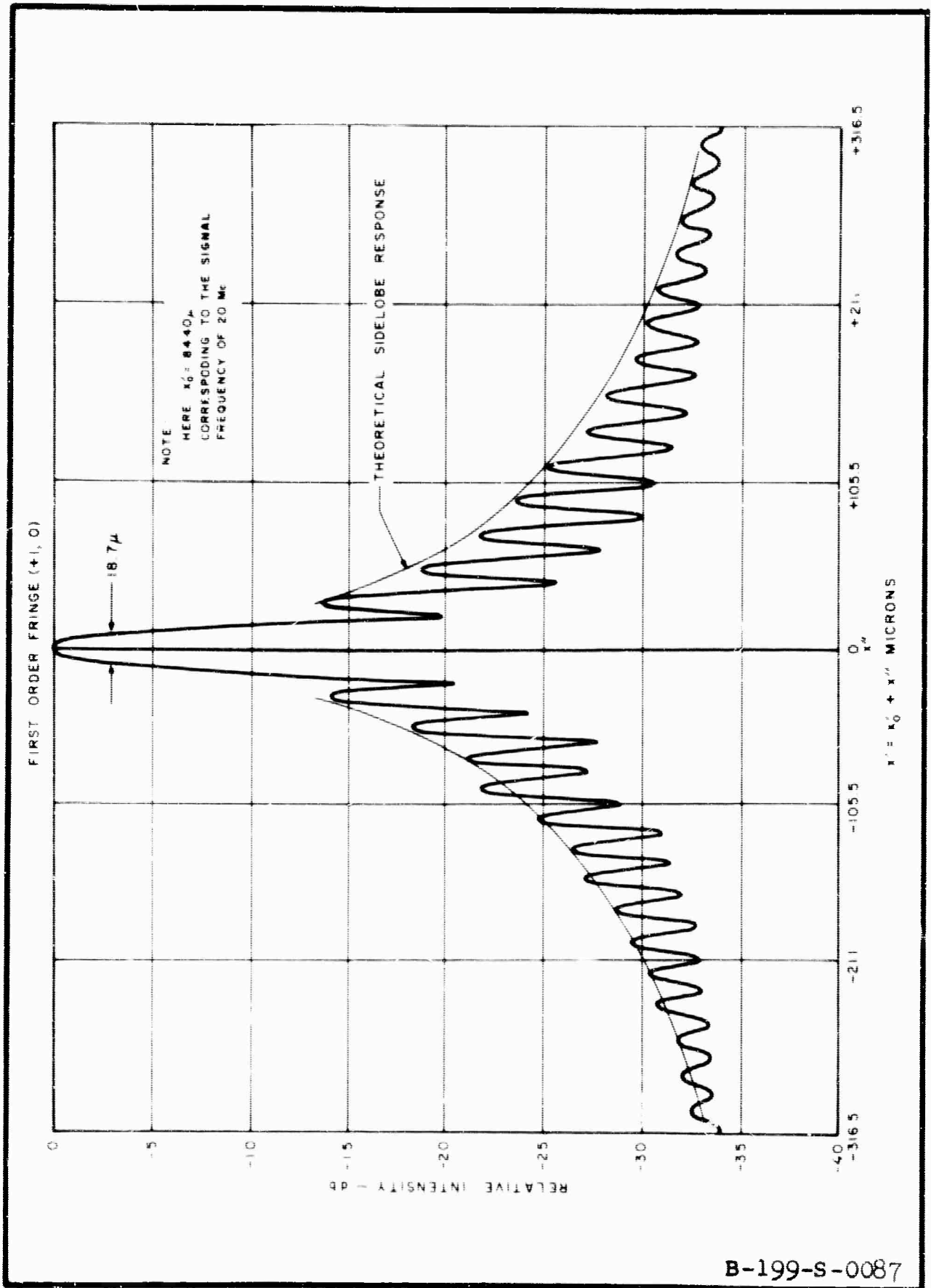THE OUTPUT FOCAL PLANE (MAGNIFICATION x 100)

B-199-S-0087

Fig. 10 Experimental First Order (Signal) Light Intensity Distribution In Output Focal Plane - x' Dimension

fringe for a uniform amplitude aperture distribution in the input focal plane. The top photograph was taken at an exposure time of 1/50 second. The peak intensity of the (+ 1, 0) (+ 1, + 1) and (+ 1, - 1) fringes is visible but the sidelobes are very faint. The bottom photograph, taken with an exposure time of 1 second, shows the sidelobes very clearly.

Figure 9b shows the same set of fringes with the aperture amplitude weighted by the distribution shown in Fig. 7. The sidelobes, in the y' direction are clearly suppressed.

Figure 10 shows the experimental light intensity distribution of the (+ 1, 0) fringe along the (x¦0) axis. The sidelobe response is very nearly ideal but the depth of the nulls shown indicates that some phase error is introduced by the lenses in the system. Note that a direct correspondence exists between the x' coordinate and the signal input frequency. From Eq. 6b this relation is given by

$$x' = \frac{\lambda_L F}{S} f_o \qquad (17)$$

For the parameters of this system, 1 μ along the x' axis corresponds to 2.37 KC in frequency.

Figure 11 shows the light intensity distributions of the (+ 1, 0) and (+ 1, $\pm$ 1) fringes along the (x' = 8440 μ, y') axis. The y' axis is marked in both actual distance and target angle sine values. The (+ 1, $\pm$ 1) fringes therefore correspond to the back lobe of the antenna. For this recording all 24 transducers were operated in parallel. This is the condition for an on-boresight target signal and a uniform amplitude aperture distribution.

A comparison of Figs. 10 and 11 with Figs. 5 and 6 shows that the first order and the zero order light distributions
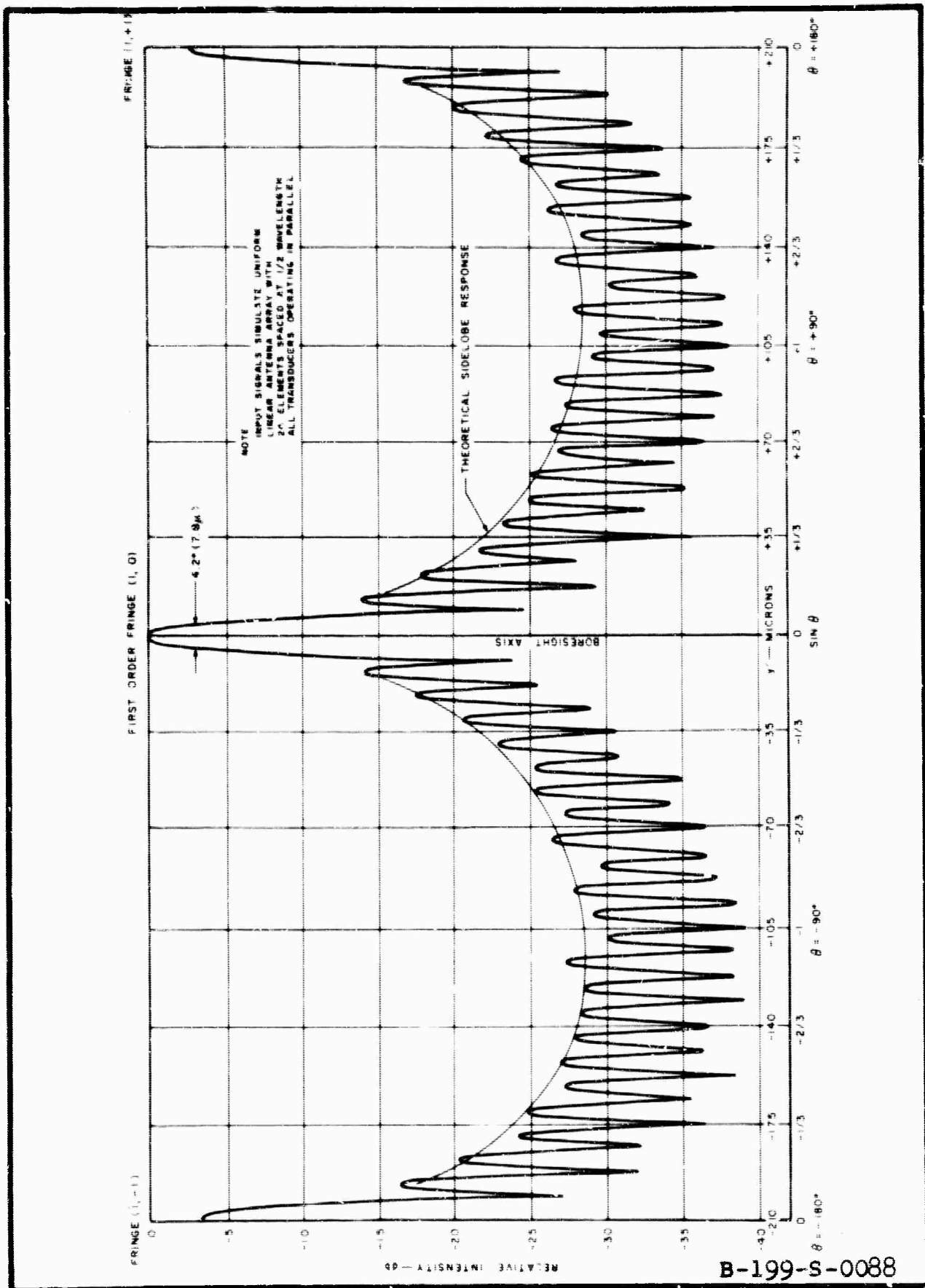
Fig. 11 Experimental First Order Fringe Light Intensity
Distribution In Output Focal Plane

are the same. This indicates that the ultrasonic modulator does not degrade the processor response.

Figure 12 depicts the first order fringe light intensity distribution along the y' axis when the aperture is amplitude weighted as shown in Fig. 7 and the phase distribution is uniform (target on boresight). The theoretical sidelobe level is 31.6 db but the experimental results indicate that only 28 db was obtained. A comparison of Fig. 12 and Figs. 6 and 11 shows that the sidelobe level only decreases to the null levels obtained for the uniform amplitude case. This seems to suggest that the sidelobe suppression is limited by phase errors introduced by the optics of the system. The variations in the sidelobes also indicate that small phase and amplitude errors exist in the ultrasonic modulator input signals; these, however, would not be responsible for increasing the sidelobes near the main lobe.

Figures 13, 14 and 15 show the processor response with a weighted aperture and target signals at -9.6°, $+41.8^\circ$ and -19.5° off the boresight axis. Again the sidelobe level obtained is very nearly limited by the null depth of the uniform aperture response.

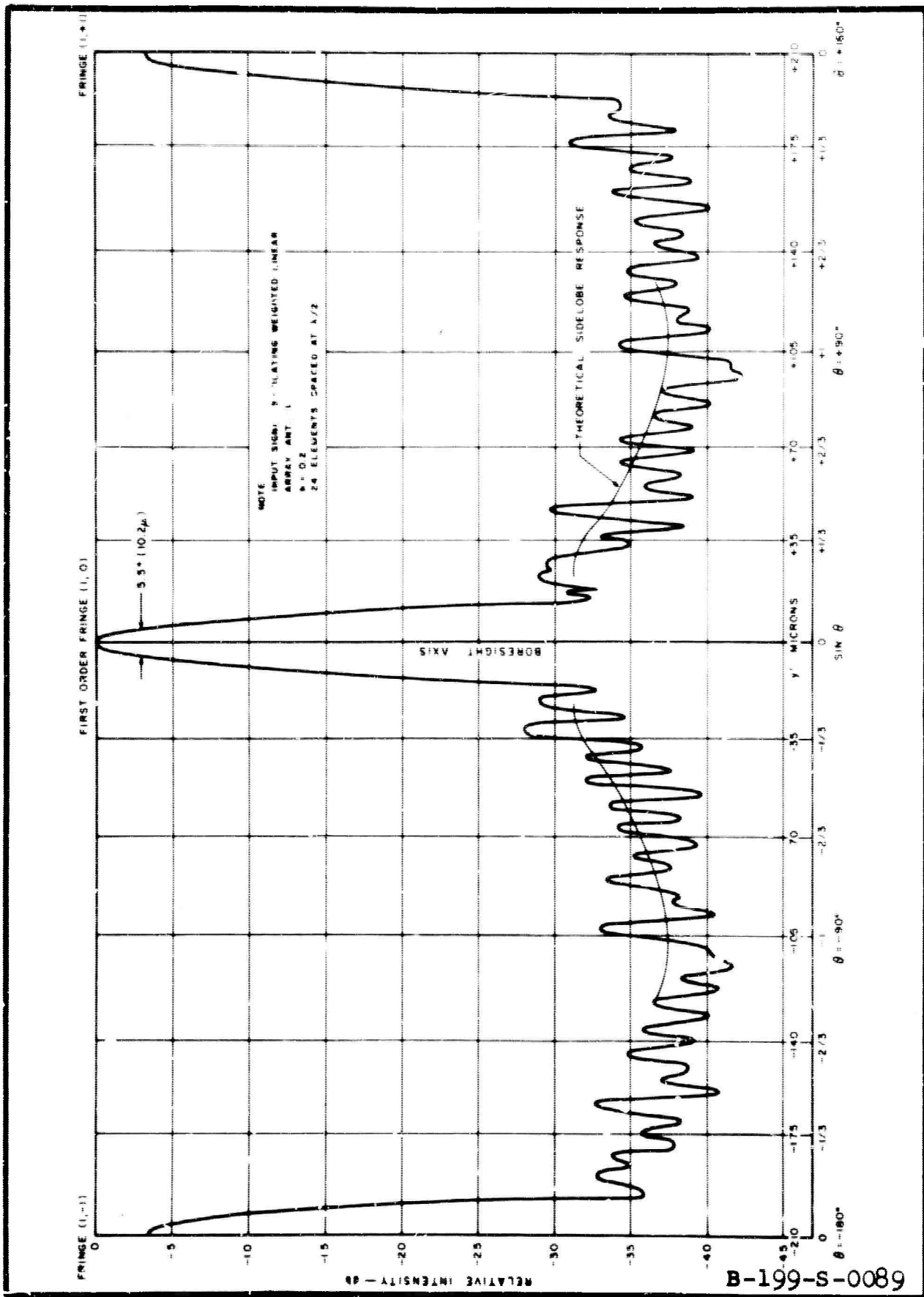Fig. 12 Experimental First Order Fringe Light Intensity Distribution In Output Focal Plane - S stem Response To Signal On Boresight
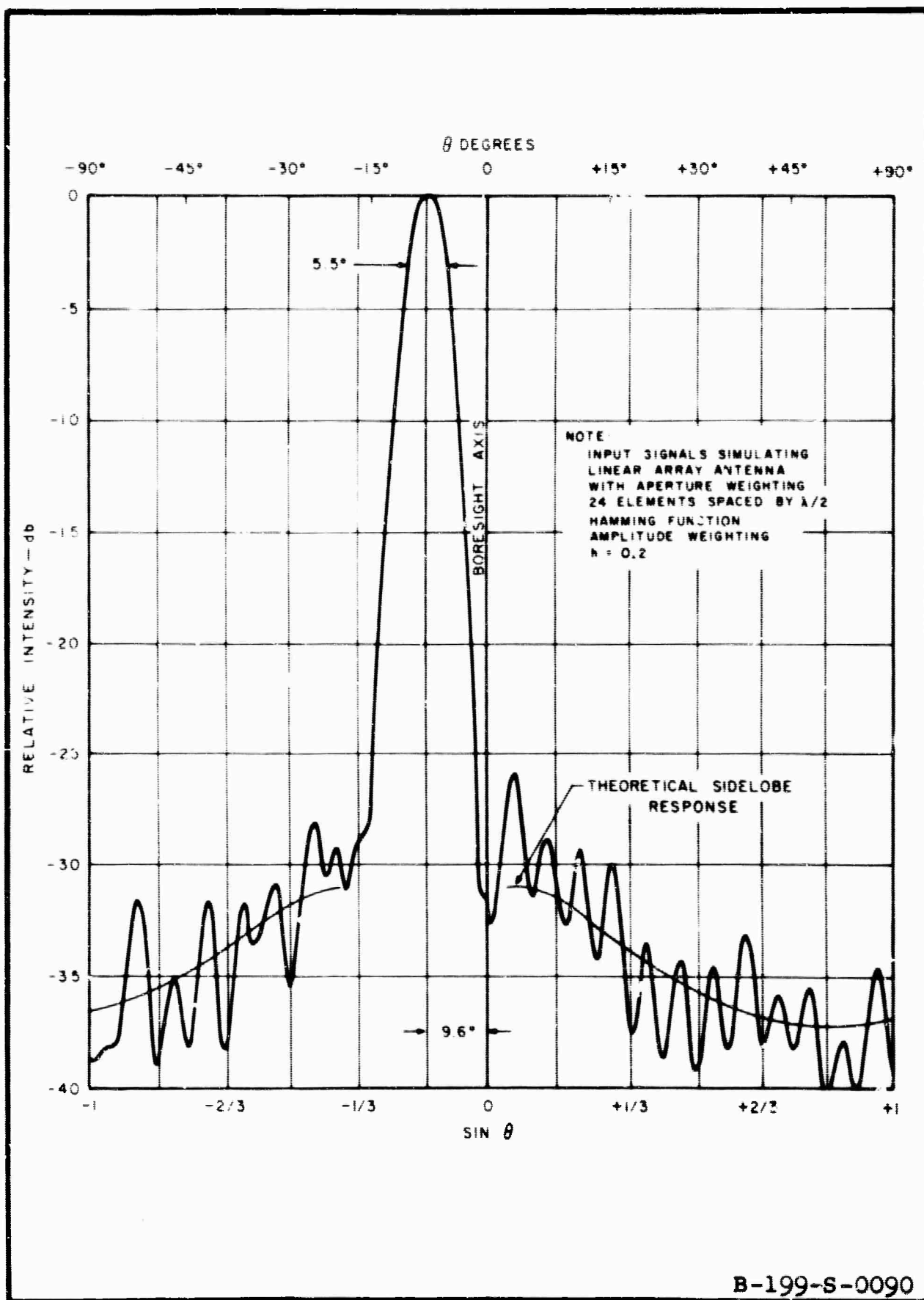
Fig. 13 Measured Output Response For Signal At -9.6°
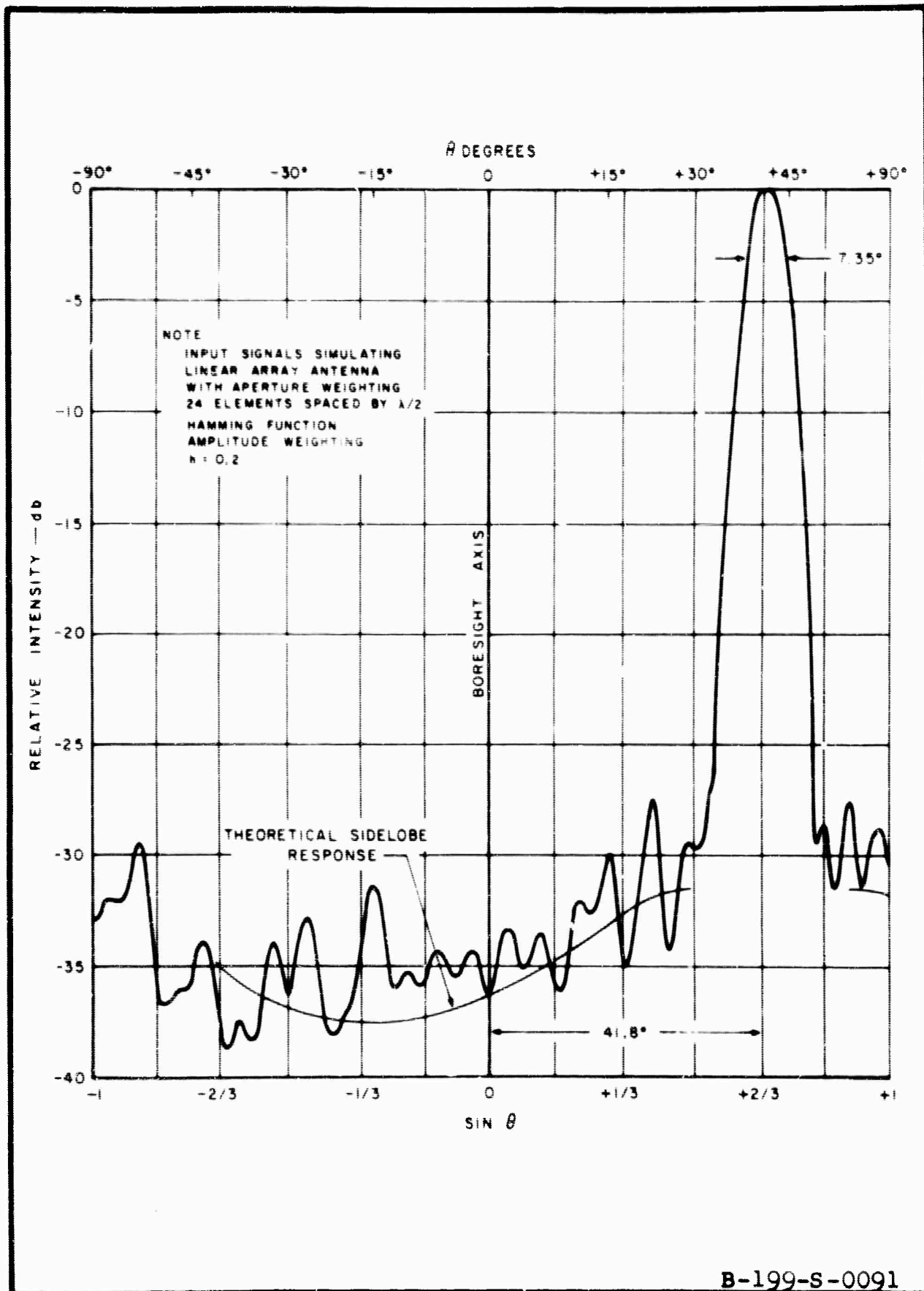Off Boresight With Sidelobe Suppression

Fig. 14 Measured Output Response For Signal at +41.8°
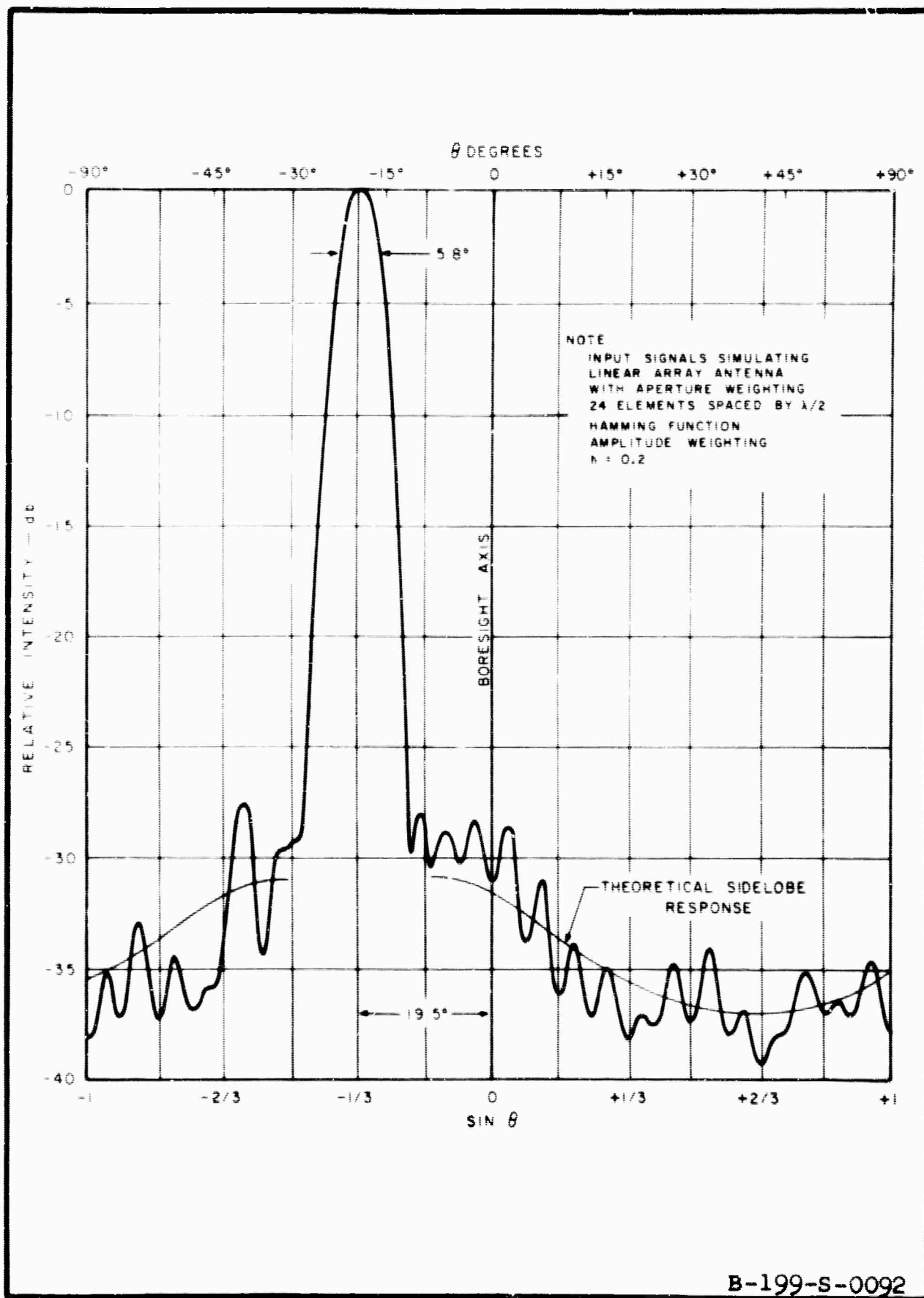Off Boresight With Sidelobe Suppression

Fig. 15 Measured Output Response For Signal At -19.5° Off
Boresight With Sidelobe Suppression

III.   SIGNAL SIMULATOR FOR TIME DELAY MULTIPLEXED SYSTEM

In order to experimentally determine the detailed charac-
teristics of the time-delay multiplexed processor, an input
signal is required which essentially simulates the output of
a linear antenna array. The signal simulator is required to
produce a train of carrier pulses whose relative phase delays
can be controlled, so as to simulate various angular target
locations.

In the time-delay multiplexed technique, the signals re-
ceived from one target by each element of an M element
phased array are heterodyned to an intermediate frequency,
appropriately delayed, and then summed with all other element
signals to form a pulse train. Thus a single waveform is con-
structed from an ensemble of pulses. In the electro-optical
processor, this pulse train acts as the input signal to a
single channel, ultrasonic light modulator. The equation of
the pulse train has been derived[1-5] as

$$V_s(t) = \sum_{n=-\frac{M-1}{2}}^{n=+\frac{M-1}{2}} P_T(t-nT) \cos [2\pi f_0(t-nT) - n\pi \sin \theta]$$

where:

$$P_T(t-nT) = \begin{cases} 1 & \text{for } |t-nT| \leq T/2 \\ 0 & \text{for } |t-nT| > T/2 \end{cases}$$

M = number of elements in linear antenna
array whose output is simulated.

n = array element index *

T = pulse width

f_o = intermediate carrier frequency

θ = angle of target off-boresight axis
of linear antenna array.

This is a signal of overall duration MT sec, containing M
carrier pulses of width T repeated every interval T (ap-
proximately 100 per cent duty cycle) such that the phase of
the carrier in a given pulse lags the phase of the carrier
in the preceding pulse by $\pi \sin \theta$, corresponding to a time
lag $(\sin \theta)/2f_o$. The values selected for the simulator were:
$M = 24$, $T = 0.8$ microseconds, $f_o = 20$ megacycles.

A. BLOCK DIAGRAM

The block diagram of the simulator has been revised to
show the physical separation between multiplex channels. See
Fig. 16.

We are using 12 channels to simulate the reception of
24 linear array antennas. This is possible if the total de-
lay of 12 channels is a multiple of the carrier period $1/f_o$.
Then the phase pattern from antenna element 13 to element
24 is a repetition of the pattern from element 1 to element
12.

A Master Oscillator simultaneously triggers a Digital
Clock and a Frequency Multiplier. The Digital Clock produces
clock pulses of period 0.8 μsec, corresponding to the pulse

---

* For M even, n is not an integer, but assumes the values:
$n = \pm \frac{1}{2}$, $\pm \frac{3}{2}$, ... $\pm \frac{M-1}{2}$, varying in integral steps.
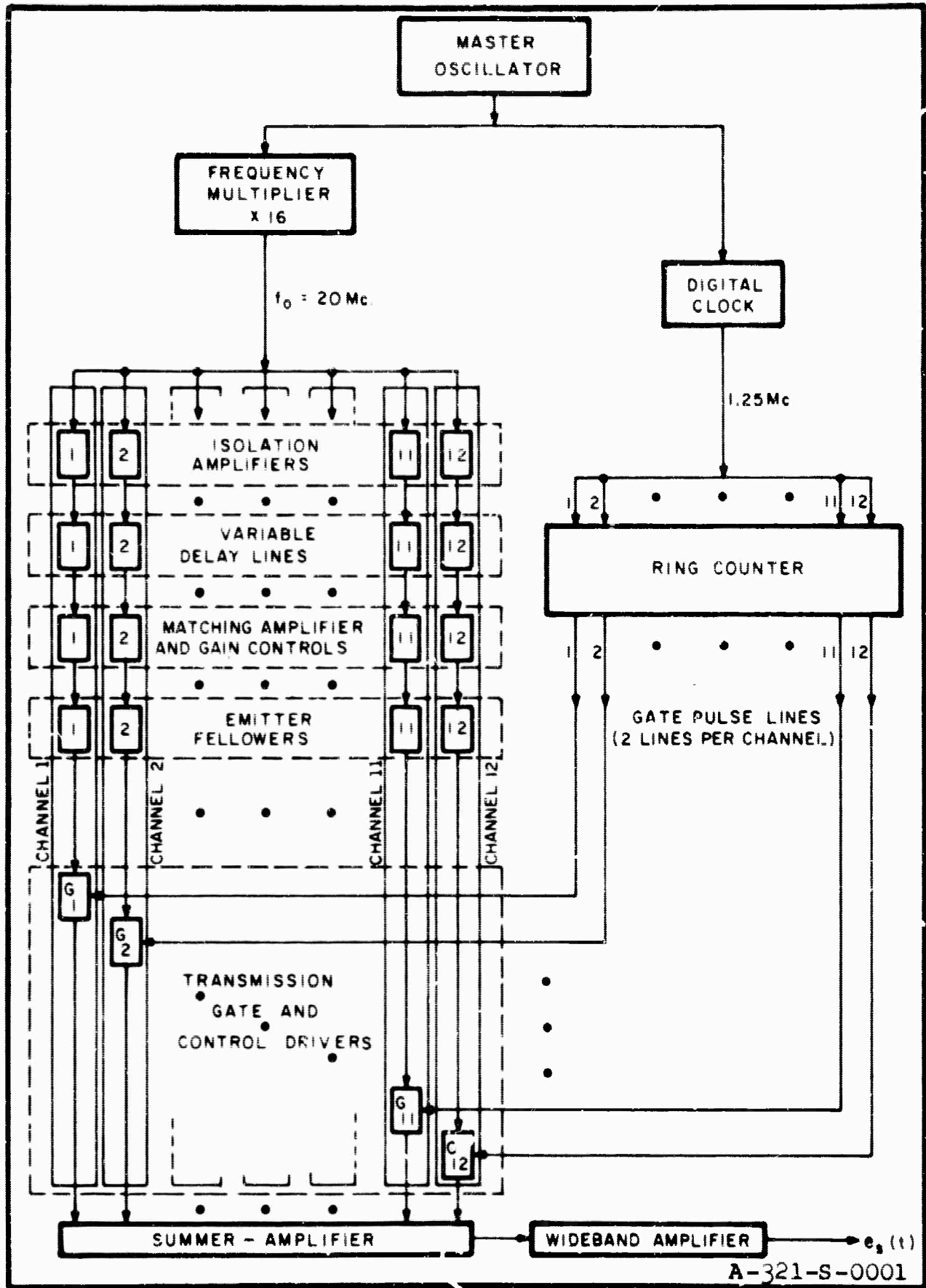
Fig. 16 Block Diagram Of Signal Simulator To Generate
A Time-Multiplexed Waveform

width T. The Frequency Multiplier generates the 20-mc carrier f_0 by a ×16 multiplication. The carrier is multiplexed to 12 identical, numbered channels. Each channel contains a delay line and a transmission gate. For a given target angle θ between 0 deg and 90 deg the carrier in channel M (M = 1, 2 ....12) may be delayed relative to channel M-1 by $\sin \theta/2f_0 = \sin \theta/40(10)^6$ sec, corresponding to the required phase lag $\pi \sin\theta$. The phased carrier appears at the input to the transmission gate.

Meanwhile, the Digital Clock drives a Ring Counter. The output lines of the Ring Counter are pulsed one at a time in numerical sequence. After the 12th line is pulsed, the cycle is repeated. Each pulse, called a Gate Pulse, is 0.8 μsec wide, corresponding to the period of the digital clock. These pulses turn ON the Transmission Gates in numerical sequence, one at a time. In the absence of a Gate Pulse, the Transmission Gate is OFF. When the gate is ON, the phased carrier at its input is transmitted to the SUMMER-AMPLIFIER, which sums all the gate outputs. The resulting signal $e_s(t)$ differs from the required $V_s(t)$ only in that $e_s(t)$ is not of finite duration MT, but is continuous.

B. IMPLEMENTATION

Described herein are the functional blocks not previously discussed.

In order to drive 12 Isolation Amplifiers from the single-ended Frequency Multiplier, it was found practical to terminate the multiplier in a simple matching section. See Fig. 17. This was possible because the unloaded output signal of the multiplier is large (doubler stages have gain) while the multiplex channels (also having gain) require a low input signal. This matching section yields a Q of 10 for good tuning of the final doubler stage of the multiplier. Neglecting large $C_0 (C_2 \langle \langle C_0)$, the design equations become:
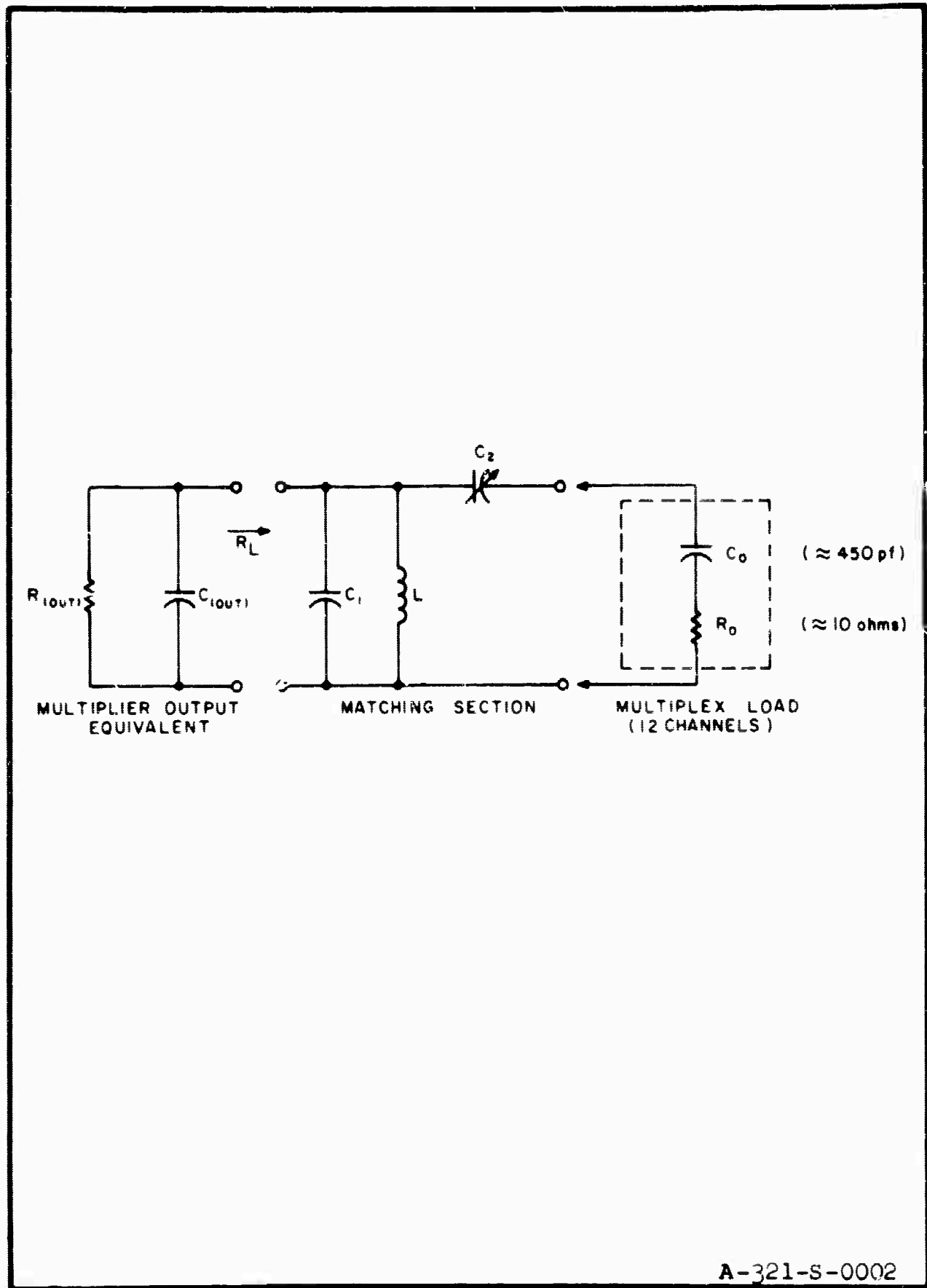
A-321-s-0002

Fig. 17 Multiplex Coupling

$$C_1 + C_{(OUT)} \approx \frac{Q}{\omega_o R_p} - C_2 \left(\frac{1-R}{R_p} Q \right) \qquad\qquad \omega_o = 2\pi \times 20(10)^6$$

$$R_p = \frac{R_L R_{(OUT)}}{R_L + R_{(OUT)}}$$

$$R_L = \frac{(E_p)^2}{2p_o} \qquad \text{where: } E_p = \text{optimum peak voltage swing of final Multiplier stage}$$
$$p_o = \text{power output}$$

$$L = \frac{R_p}{\omega_o Q}$$

$$C_2 = \frac{1}{\omega_o R_o \sqrt{R_p/R_o - 1}}$$

To sum the transmission gate outputs, all that is required
is a resistor. Since only one signal is gated at a time, no
analog addition circuitry is required. The outputs are all
tied together. Then the energy stored in the output capacity
when one gate turns OFF is rapidly dispelled in the low output
impedance of the gate which simultaneously switches ON, and
the new carrier phase is quickly established. Output capacity
should be minimized, and matching is required to the commercial
wideband amplifier. A matching amplifier accomplishes both.

C. PHASE ALIGNMENT OF SIGNAL SIMULATOR

Were it possible that all the phased carrier signals be
exactly in phase, and that there be zero delay between turn off
of one transmission gate and turn on of the next, then the sum-
med output $e_s(t)$ would be a pure carrier. Its frequency spec-
trum would be a line at 20 mc. If the phases are not all alike,
the phase is time-variant. The phase variance is repeated every
12 pulses, so that the repetition frequency of this phase error
distribution is $1/12 \times 0.8$ µsec = 104 kc. The frequency spec-
trum detects phase errors by showing lines at frequencies dis-
placed from 20 mc by multiples of the phase variance repetition

frequency. These "sidelines," located at 20 mc ± K104 kc ($K = 1, 2, \ldots\ldots$), must be minimized.

Phase alignment was performed using the AD-YU Precision Phase Meter Type 205A-1-2. The instrument is a sensitive phase comparator with a calibrated delay line. The phase between two inputs is read on the delay line dial when by adjustment of amplitude and delay a null is detected. Zero phase is defined as the dial reading at null when a reference signal is compared with itself. When another signal is compared with the reference, and a null obtained at a new dial reading, that phase delay between the two signals is the difference between the new dial reading and the zero reading.

For zero-phase alignment, the reference signal is f_o. The phase of the summed output signal $e_s(t)$ is compared with f_o when one transmission gate is always ON and all other gates are always OFF. A switch is provided in each Gate Pulse Line to render the corresponding transmission gate always ON, always OFF, or GATED. The output $e_s(t)$ will reproduce the phased CW signal at the input to the ON gate. The delay line and gain control in the ON channel are used to null the meter. If such a null is produced at the same meter dial setting for all channels, then all the channels are in phase.

The alignment was checked with a Proboscope Spectrum Analyzer. The first "sidelines" were 30 db below the amplitude of the 20-mc line, and the second "sidelines" were down 35 db.

Next the channels were aligned for a total antenna delay of two periods of the carrier, or 100 nanoseconds. The delay between adjacent channels was then $100/24 = 4.17$ nanoseconds. The phase repeats every cycle of the carrier, or every 12th pulse, and the phase distribution repetition frequency is $1/12 \times 0.8$ μsec = 104 kc.

This is accomplished as follows: Terminals exist on the rear of the phase meter for connecting an external delay line in series with the internal delay line. We set the required 4.17 nanosec on the internal delay line and store the total delay in the external delay line. This is necessary because equal delay increments set on different parts of the internal delay dial are not equal in actual delay. With this method we operate on a fixed portion of the dial. In practice, Channel 1 is gated ON with all other gates OFF. The internal dial is zeroed by comparison of identical signals. The reference signal is multiplex input f_o. The internal delay dial is set to its zero position, e_s is compared with f_o, and the external delay line is adjusted to null the meter. The internal delay dial is now advanced 4.17 nanosec. Channel 1 is turned OFF and Channel 2 turned ON. Output $e_s(t)$ is compared with f_o, and the variable delay line and gain control in Channel 2 are used to null the meter. The internal delay dial is returned to its zero position and the external delay line is adjusted to restore the null. Thereby, Channel 2 is delayed 4.17 nanosec with respect to Channel 1, and this delay is stored in the external delay line. The process is repeated for channels 3 to 12. As a check, after adjusting Channel 12, 4.17 nanosec is added to the external delay line, whereupon Channel 1 should null at the zero setting of the internal delay dial.

The spectrum analyzer again checks the accuracy of these settings. With all paths GATED, the output $e_s(t)$ is a continuous pulse train modulated approximately by a continuous phase ramp (actually a staircase function). For such a time signal, the line in the frequency spectrum, which was at 20 mc for the zero-phase case, will now be displaced 104 kc down to 19.896 mc. The "sidelines" indicating errors in phase or fre-

quency now appear displaced from 19.896 mc by multiples of 104 kc. As viewed on the spectrum analyzer, the first sideline was found to be 30 db below the level at 19.896 mc and the second sideline was 35 db down.

If the carrier frequency is not exactly 20 mc, the slope of the phase ramp will not be continuous at phase repetition points, and the sidelines will rise. After adjusting the frequency of the Master Oscillator for minimum sidelines, the Oscillator frequency should remain stable.

IV. REFERENCES

The following reports were prepared at the Electronics Research Laboratories, School of Engineering and Applied Science, Columbia University, New York, New York 10027.

1. Arm, M. and Lambert, L., "The Theory and Physical Constraints of an Electro-Optical Signal Processor for Phased Array Antennas," Technical Report T-1/199, October 1, 1963, Unclassified.

2. Aimette, A., Arm. M. and Lambert, L., "Electro-Optical Signal Processing Techniques for Phased Array Antennas," Progress Report P-1/199, January 1, 1964, Unclassified.

3. Aimette, A., Arm, M. and Brown, D., "Electro-Optical Signal Processing Techniques for Phased Array Antennas," Progress Report P-2/199, April 1, 1964, Unclassified.

4. Aimette, A., Arm, M. and Wyman, N., "Electro-Optical Signal Processing Techniques for Phased Array Antennas," Progress Report P-3/199, July 1, 1964, Unclassified.

5. Aimette, A., Arm, M. and Wyman, N., "Electro-Optical Signal Processing Techniques for Phased Array Antennas," Progress Report P-4/199, October 1, 1964, Unclassified.